**ORIGINAL ARTICLE**

# Dam break study and its flood risk in Gurara watershed-Nigeria under varied spatio-temporal conditions by integrating HSPF and HEC–RAS models

Al-Amin Danladi Bello[1] · Abdullahi Sule Argungu[1] · Aminu Tijjani Soron Dinki[1] · Abdullahi Yahaya[1] ·
Khalid Sulaiman[1] · Abdulrazaq Salaudeen[2] · Nura Abdullahi[1]

## Abstract

This study focuses on the flood disaster and risk that can potentially occur in the event of a dam break in the Gurara watershed, Nigeria. The aim is to evaluate the effects of land use and land cover (LULC) and hydroclimatic variability on the aforementioned dam. This is done through integration of Hydrological Simulation Fortran Program (HSPF), hydro-dynamic models and field observations. The simulation result presents the extent of the flood downstream, which inundates 274.6 Km$^2$ (27,460 ha) of the watershed, that includes a peri-urban *Jere* town with a total population of 9912 and 6000 ha of irrigation area that has the potential to produce 100,000 metric tons of food in four circles per year. Further analysis of the result shows that the flood hazard map of the flooded area produced a varied index for each scenario, but it shows that the hazards increase with an increase in the literal inflow into the dam from the upstream runoffs. The hazard maps identify risks in vulnerable areas. The downstream area experiences diverse exposure based on the proximity of LULC class to the prone zones. This research presents details about the possible disaster associated with dam collapse in nearby communities.

**Keywords** Gurara dam · Watershed · HSPF model · Dam break · Flood risk

## Introduction

Over the course of the past 7 decades, sub-Saharan African nations have undergone a consistent rise in occurrences of inundation, which have had a persistent impact on both societal and economic facets across various magnitudes (Tramblay et al. 2020). More people might be affected by these events than by any other form of natural hazard (Rentschler et al. 2022). To mitigate the peril of flooding, water control infrastructures are usually provided, such as dams, detention basins, etc., to attenuate the excess flood (Polemio and Lollino 2011). Nigeria's floods are caused by uncontrolled urban growth and insufficient infrastructure, which worsens the effects on urban areas. Even floods occurring in rural areas still harm human populations and agro-economic activities (Aboyeji 2016). In recent decades, there has been a significant influx of people and uncontrolled changes in land use in many countries. These changes have caused significant climatic and hydrological shifts that have greatly impacted the availability and distribution of water resources worldwide (Song et al. 2018).

Therefore, most watersheds in Nigeria are not exempt. For example, the Gurara catchment has a multipurpose dam called the Gurara dam which holds eight-hundred and eighty-million-cubic-meters of water. This dam serves three purposes: conveying raw water to the Usuma dam, transferring water to a hydro power station, and irrigating a six-thousand-hectare land area at Azare. The existence of the Gurara dam led to a consecutive increase in the activity level within the watershed, and as a result, tremendous and unplanned changes were recorded between the years 2000 and 2020, with an increase in built-up area recording one of the highest percentage increases for decades. Before the construction of the dam, the lower Gurara watershed usually experienced flooding on an annual basis (Dam et al. 2003).

✉ Al-Amin Danladi Bello
adbello@abu.edu.ng

1  Department of Water Resources & Environmental Engineering, Faculty of Engineering, Ahmadu Bello University, Zaria, Nigeria

2  Department of Civil Engineering, Faculty of Engineering, Abubakar Tafawa Balewa University, Bauchi, Nigeria

However, the existence of the dam prevents the recurrence of flooding at the lower Gurara watershed. But evaluating the ability of the dam to sustain the attenuation of the excess floods under varied spatio-temporal conditions is important.

As expected, increased flood occurrences will be consistent over the years due to human activities and climate change that is consequential to global warming (Serdeczny et al. 2017). It is crucial to evaluate the Gurara dam's ability to reduce flood damage and its impact on the lower Gurara watershed if it fails. Flood-induced dam failures are a severe environmental danger that affects ecological systems, socioeconomic factors, and human lives (Li et al. 2019). Several studies indicate that the processes leading to dam failure can be ascertained from past dam failures (Lyu et al. 2019). Hence, scientists have proposed several numerical models to predict dam failure based on the historical failures of over 180 dams (Xu and Zhang 2009; Zhang et al. 2009). The escalation of dam failures worldwide is expected due to climate change and human activities. (Ghimire et al. 2022; Kim and Sanders 2016). Forecasting flood conditions is crucial in selecting dam sections for watersheds. Many dams intercept floods greater than their intended flood hydrograph due to climate and human activities (Piciullo et al. 2022). The dam's behavior and operation may be affected by conditions, which could lead to dam breaches. Assessing flooding hazards and risks downstream and in the lower watershed is necessary for effective management and prevention of losses. Modeling techniques are commonly used to predict dam failure parameters, flood hydrographs, and extents.

There are various methods to determine the flood inundation caused by dam failures derived from the amplification of runoff due to excess rainfall (Nastiti et al. 2015; Elfeki et al. 2017; Abdessamed and Abderrazak 2019; Davenport et al. 2020, Tedla et al. 2021). According to Mudashiru et al. (2021), flood inundation modeling requires the integration of semi-distributed and other related numerical models that have the capacity to capture both the hydrologic and hydraulic behavior of the proposed study area. This approach has considerably provided historical, real time, and future flood conditions at regional (Gouldby et al. 2008), large or small watersheds (Toosi et al. 2019; Bhattarai et al. 2023), sub-watersheds (Wijayawardana et al. 2023), cities (Guan et al. 2023) and small towns (Ha et al. 2023). Most studies emphasized the evaluation of the impact of floods under extreme rainfall and anthropogenic impacts for a critical understanding of flood behavior (Guo et al. 2021). However, these studies are concentrated in developed regions, such as the USA, Canada, China, etc., whereas in sub-Saharan African regions, similar studies are hardly conducted due to scarce data, a lack of adequate information, and other related problems (Nkwunonwo et al. 2020). However, a method that combines GIS technology and boundary conditions to simulate the hydrological processes of the watershed has proven

to be not only economical but accurate in producing a comprehensive evaluation of the watershed processes (Salaudeen et al. 2023). This study is unique, because it integrated watershed modeling in a data-limited environment and conducted site-based risk evaluation in an informal community, distinguishing it from other similar studies. Watershed models simulate the natural processes that occur in a watershed, such as flow of water, sediments, chemicals, nutrients, and microbial organisms, and evaluate quantitatively and qualitatively the impact of anthropogenic activities and changing land systems on these processes (Kumar et al. 2021). There are several numerical models accessible for flood inundation modeling. Among these, the hydrological simulation program FORTRAN (HSPF) and hydrodynamic model—Hydrologic Engineering Center–Rivers Analysis System (HEC–RAS)—are selected to conduct this study. The HSPF model is one of the best hydrological models used to evaluate the rainfall–runoff interaction at various watershed scales (Kovalenko et al. 2022). In addition, for hydrodynamic modeling, the HEC–RAS model is a very important tool for flood inundation studies (Namara et al. 2022), dam breaks (Amini et al. 2022), and the design of hydraulic structures (Açıl et al. 2023; Zaborowski et al. 2023). Among the advantages of the 2D coupled HEC–RAS model is its ability to simulate flood extents and the time likely to occur (Dasallas et al. 2019). With these facts, HSPF and HEC–RAS are adopted in this study.

# Materials and methods

## Study area

The Gurara watershed is located in the northern part of Nigeria, between latitudes 8°15′ N and 10°05′ N and longitudes 6°30′ E and 8°30 E, and has a total catchment area of 4352 km$^2$. The basin is tailored in a north–east–south–west direction, with its headwaters starting from the western side of the Jos plateau. The watershed is centered between the semi-arid north and the sub-humid climate in the south, and its climate is characterized by dry northern winters and wet northern summers. There are two major seasons experienced in the watershed, which are the wet and dry seasons. The dry season lasts between November and March, while the wet season begins in May and lasts until October (Oseke et al. 2021). The vegetation is savannah grassland with a sparse distribution of tropical forest. The terrain is undulating and dissected, with clay-loam soil and red laterite/alluvial soil being the prevalent soil types. The mean annual rainfall at the location is 1400 mm, and the mean monthly maximum and minimum temperatures in the catchment are 37.3 °C and 19.7 °C, respectively. There are five hydrological stations located within the watershed, namely, Gantan, Izom,

Jere, Kachia, and Kurmin Musa, as depicted in Fig. 1. The watershed houses the popular Gurara Dam, which is located in the mid-section in between the mountainous region of high terrains that characterized the uniqueness of the Gurara River and the low savannah downstream. Table 1 shows the general characteristics of the dam.

## Brief models description

*HSPF model* The Hydrological Simulation Program Fortran (HSPF) is a comprehensive, semi-distributed watershed model supported by the United States Environmental Protection Agency (USEPA). It is used for the simulation of hydrological, environmental, and water quality-related processes of different sizes and complexities (Kovalenko et al. 2022). The model has three main modules: the pervious, known as PERLAND, the impervious, known as IMPLAND, and the reaches, referred to as RCHRES, which are used in simulating pervious land segments, impervious land segments, and free-flow reaches, or mixed reservoirs, respectively.

**Table 1** Gurara dam characteristics

| Dam Characteristics | Details |
| --- | --- |
| Reservoir area at NWL | 55.4 Km$^2$ |
| Total reservoir capacity at NWL | 882 Mm$^3$ |
| Dead storage at MOL | 175 Mm$^3$ |
| Active storage | 707 Mm$^3$ |
| Dam type | Rockfill |
| Total length of top of dam | 3250 m |
| Embankment dam with 3 different sections | Rockfill, random fill and transition dam |
| Maximum height above foundation | 55 m |
| Total volume | 788Mm$^3$ |
| Upstream face slopes H/1 V | 1.6 (rockfill) |
| Downstream face slopes H/1 V | 1.5 (rockfill) |

The model routes water from one reach to another using the storage routing technique and explains hydrological
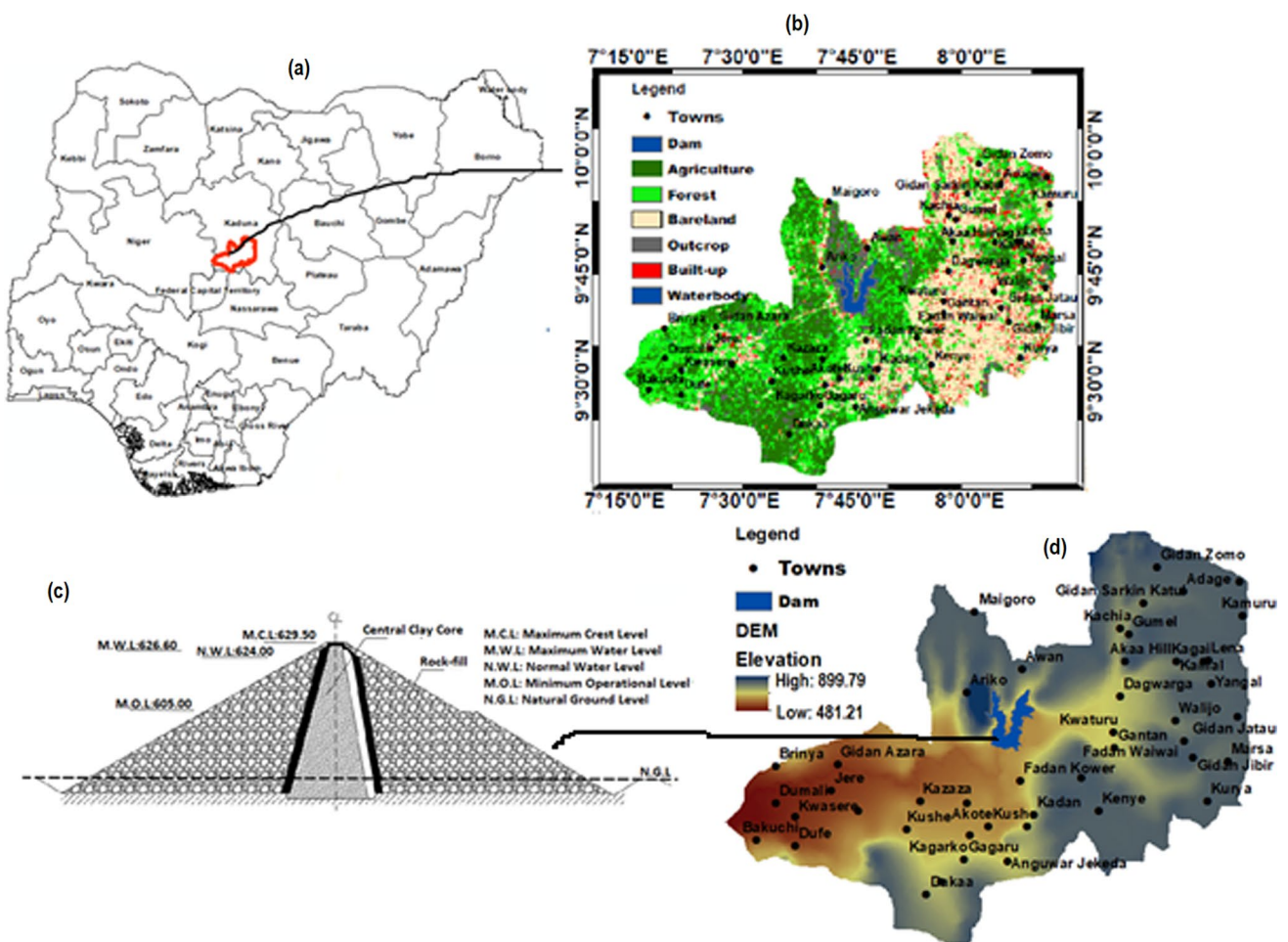


**Fig. 1** **a** Geographic location of the study area **b** elevation details of Gurara watershed. **c** Land-use/land-cover characteristics. **d** Cross-sectional details of Gurara dam

behavior using the kinematic wave technique. In addition, the hydraulic characteristics of reaches are defined in the function tables provided by the model, and the effects of vegetation type, density, root growth, stage development, and soil moisture are all lumped into the LZETP module.

The module is embedded in the Better Assessment Integrating Point and Non-Point Sources GIS software, popularly called BASINS, which fosters the delineation and sectioning of the watershed. The mathematical representation of the watershed is done by an embedded plug-in in the software known as the Watershed Data Management Program, which facilitates the preparation of the input metrological and hydrological data sets. The data sets required by the model for proper simulation are the land use and land cover information, the digital elevation model, and other data like air temperature, dew point temperature, precipitation, stream discharge, open evaporation, solar radiation, and wind speed. For calibration and validation of the model, HSPF expert system software (HSPEXP++) was used. The calibration and validation processes were carried out by adjusting parameters in accordance with the guidelines of USEPA technical note 6. The calibration and validation of the hydrological model were done using the observed stream flow. The calibration was done using the 2002–2005 data set, while the validation was done using the 2006–2009 data set. The chosen time intervals were designated on account of the inadequacy of contemporary data to accurately represent the current state of the watershed. Therefore, the utilization of hydrological modeling in this inquiry becomes imperative (Swain et al. 2020).

*HEC–RAS model* In this study, HEC–RAS software version 6.3.1 was used. The software was designed to simulate the hydraulic and hydrologic behavior of hydraulic structures and their impacts during operation or failure. It is a well-developed and tested model that has been used all around the globe. The model utilizes the energy and momentum equations derived from the 1-D/2-D Saint Venart formula for generating steady and unsteady flows using the concept of the finite difference method. This software has the capability to compute the water surface profile in steady and unsteady flow conditions, sediment digenesis, flood

extents, dam breaches, and hydraulic design. The details of the software can be further read in the HEC–RAS user manual (Brunner 2016).

## Input data

The meteorological data, such as precipitation, cloud cover, wind speed, solar radiation, dew point temperature, and evaporation, were collected from the Nigerian Metrological Agency (NIMET) and the Federal Ministry of Water Resources (FMWR). More meteorological data were downloaded from NOAA (National Oceanic and Atmospheric Administration) under the US Department of Commerce (http://www.noaa.gov/). For the daily observed streamflow records of the Gurara watershed, they were obtained from the Kaduna State Water Board and Gurara Water Development Authority. The elevation data were obtained from the Global Data Explorer (https://gdex.cr.usgs.gov/gdex/) and used for the watershed delineation. Some data points for the Gurara river are obtained from FMWR, and after it was integrated with the spatial data, a final DEM of 5 m/pixel resolution was produced, which was used in the 2D hydraulic modeling of the Gurara dam failure in the HEC–RAS model. Other spatial data, such as the land-use data, were developed from remote sensing data obtained from the United States Geological Survey (USGS) EROS Data Center via the USGS Global Visualization Viewer. The imageries were captured by Landsat 4–5 (thematic mapper) and Landsat 7 (enhanced thematic mapping) and operational land imager sensors, respectively, and were used to produce historical land-use and land-cover (LU/LC) data of the study area. While the soil map was obtained from the Federal Ministry of Agriculture (FMOA). The data used in this study, its resolution, and its sources are shown in Table 2.

## Model development

Figure 2 illustrates the procedures and steps of the model development in this study. The maximum flood hydrograph for each of the four scenarios was derived from the spatio-temporal variability of the upper Gurara watershed, which

**Table 2** Data sources and their properties

| Data type | Data name | Resolution | Sources | Period covered |
|---|---|---|---|---|
| Meteorological data | Rainfall, temperature, wind speed, cloud cover, solar radiation, and evaporation | Daily | Nigerian Metrological Agency (NIMET), FMOW, and NOAA climate data online | 1980–2010 |
| Hydrological | Streamflow | Monthly/Daily | Kaduna State Water Board, Gurara Water development Authority | 1971–1989 2001–2010 |
| Spatial | Digital Elevation Model (DEM) | 5×5 m | USGS global data explorer/depth data points | 2010 |
| Spatial | Land use | 30×30 m | Remote sensing data | 1991–2020 |
| Spatial | Soil | 1:250,000 | Federal Ministry of Agriculture | 1980 |
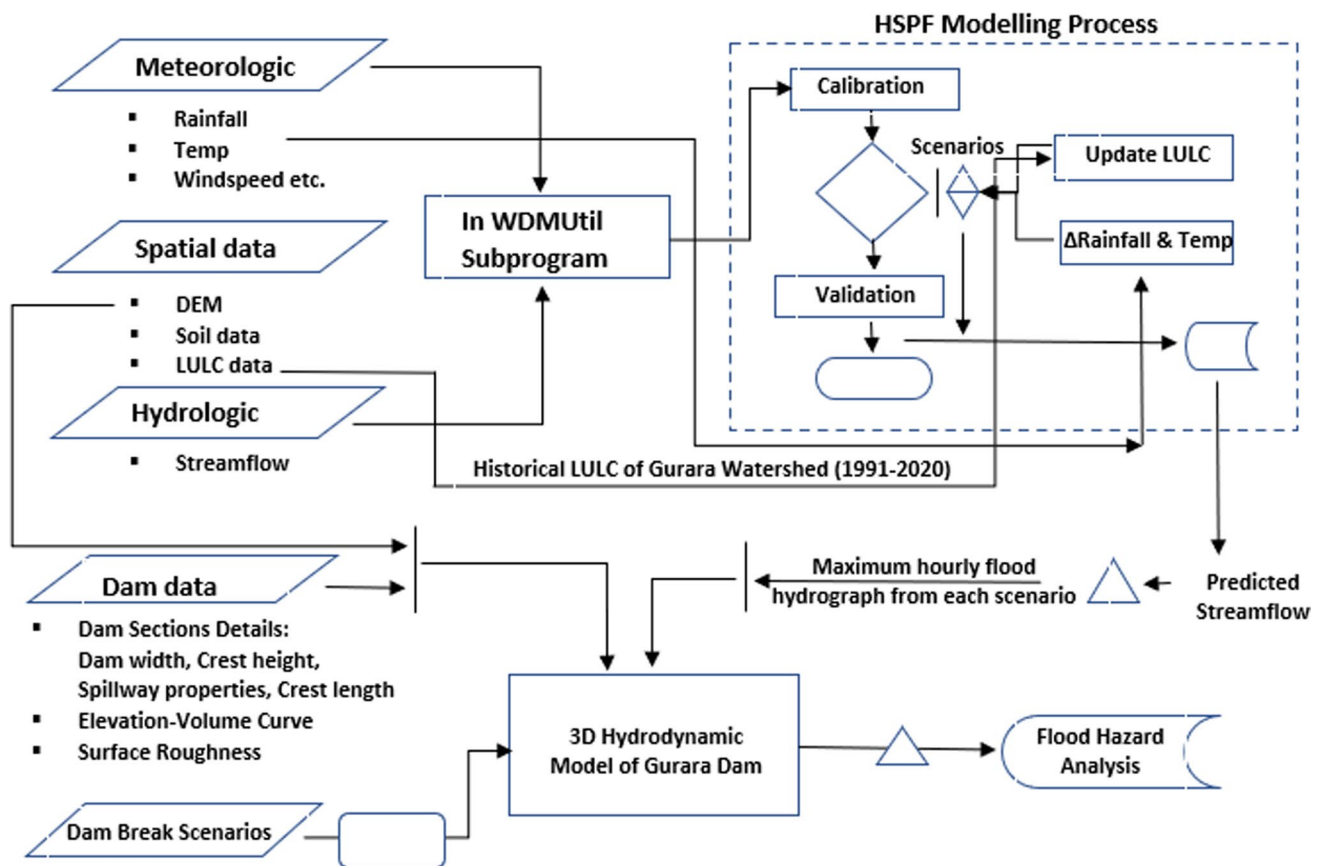
**Fig. 2** Flow chart showing Step by step model development of the study area

focused mainly on its historical land-use and land-cover (LULC) and the rainfall conditions over the span of 30 years. This was obtained from the hydrological model of HSPF. An HEC–RAS 2D model of the Lower Gurara watershed is produced to evaluate the impact of the Gurara Dam to attenuate the floods from the upper Gurara watershed and its impact at the lower section of the watershed in terms of flood hazards in case of dam failure, under different literal flood hydrographs produced from the four scenarios.

## HSPF model

The upper Gurara watershed was selected for hydrological model development, because the Gurara dam is located at the mid-section of the watershed and only runoff generated in the upper section ends up in the Gurara reservoir. Therefore, the model was calibrated by manual parameter adjustment and was further facilitated by the HSPFEXP + program. The HSPFEXP program gives multiple outputs that enable analysis of model performance. These outputs include normal plots of simulated and observed stream flow for the number of years simulated, cumulative flow, percentage of daily flow exceeded, yield duration curve, and evapotranspiration

histogram. In addition, the program generates statistical reports of the performance evaluations for the simulation runs. The available observed streamflow at the inlet of the dam at *Kachia* station extends from 2002 to 2009. The data set was sectioned into two parts: the first part used for the calibration was for a period of 4 years from January 2002 to December 2005, and the second part used for the validation was for a similar period from January 2006 to December 2009. The accuracy analysis of the model simulation showed good performance, as shown in Fig. 3.

To determine the extent to which possible climatic variations would affect the hydrology of the watershed, synthetic climate scenarios were created following the methodology of Martínez-Retureta et al. (2021), consisting of only immediate future projected precipitation and air temperature. A total of four scenarios were created, using the four historical LULC maps and the synthetic climate scenario as shown in Fig. 4. The choice of LULC temporal boundaries was predicated on a meticulous evaluation of the watershed's past anthropogenic engagements coupled with the well-established verity that the land-use and land-cover (LULC) of a region undergoes rapid transformations over a 10-year span (Moniruzzaman et al. 2020).
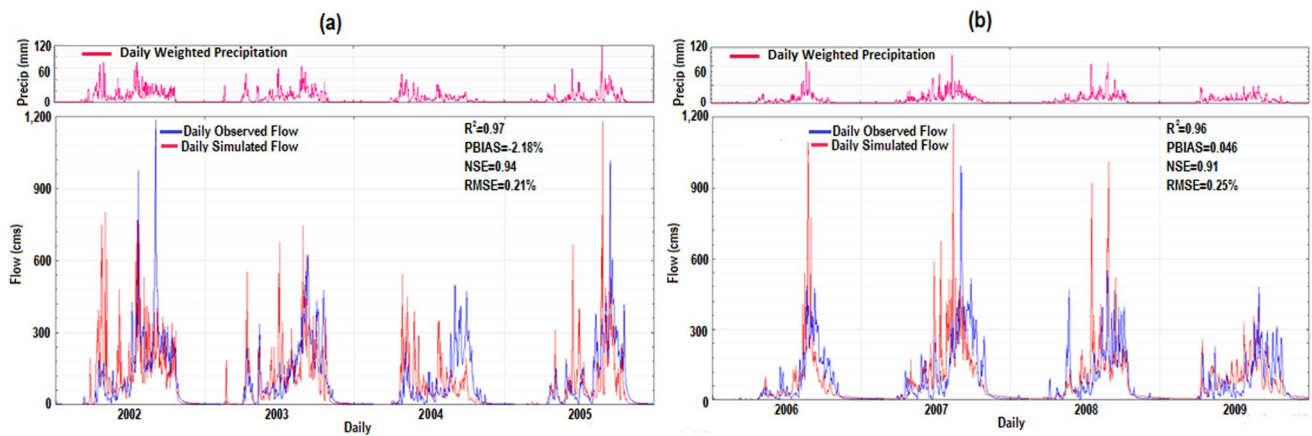
**Fig. 3** Results of the Hydrological model of upper Gurara watershed: **a** calibrated streamflow **b** validated streamflow



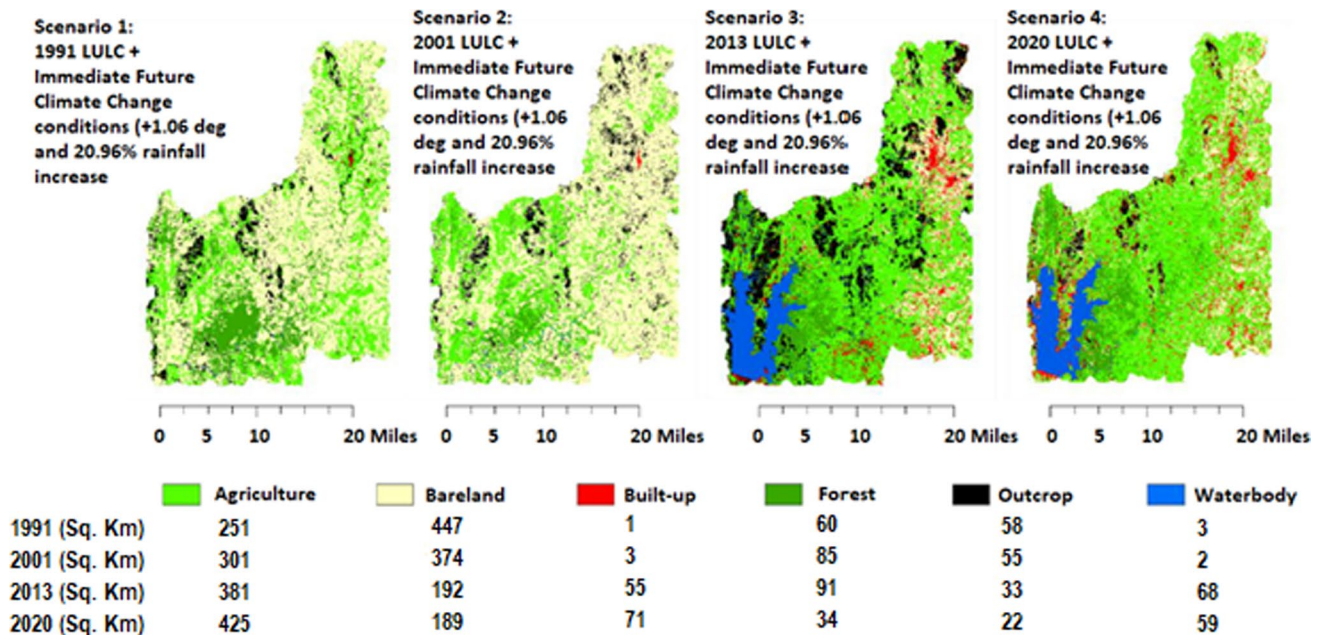| | Agriculture | | Bareland | | Built-up | | Forest | | Outcrop | | Waterbody |
|---|---|---|---|---|---|---|---|---|---|---|---|
| 1991 (Sq. Km) | 251 | | 447 | | 1 | | 60 | | 58 | | 3 |
| 2001 (Sq. Km) | 301 | | 374 | | 3 | | 85 | | 55 | | 2 |
| 2013 (Sq. Km) | 381 | | 192 | | 55 | | 91 | | 33 | | 68 |
| 2020 (Sq. Km) | 425 | | 189 | | 71 | | 34 | | 22 | | 59 |

**Fig. 4** Designed Scenarios for evaluation of excess inflows into Gurara Dam under varied spatio-temporal conditions

Afterward, the combined LULC and climate scenarios are simulated using the validated model. This study is primarily targeting maximum flood hydrographs generated from the combined effects of LULC and climate change. For the purpose of this study, the simulated scenario outputs are in hourly time-steps, different from the validated time-steps, which are on a daily basis. Statistical inference was employed to select the optimal flood hydrograph within a 24-h duration using the 95th percentile estimate using the methodology used by Bonsal et al. (2001). The flood hydrographs produced serve as flow input for the HEC–RAS 2D model.

### HEC–RAS model

HEC–RAS is a hydrodynamic model that allows one- and two-dimensional modeling by coupling steady and unsteady flow conditions to simulate the hydrologic and hydraulic behavior of natural or man-made drainage systems. In this study, two-dimensional (2D) modeling was selected due to the availability of adequate spatial data such as roughness coefficient (derived from the watershed LULC), a digital elevation model of good resolution (5 m/pixel), and hydrological information (from the hydrological modeling in HSPF) for evaluating the attenuation capacity of Gurara reservoir.

The efficiency of 2D modeling to capture the fluctuations in flood extent, its arrival, and the initiation of flooding due to hydraulic structure failure such as dams, bridges, culverts, and other retaining structures is well-documented (Urzică et al. 2021; Sarchani and Koutroulis 2022). After evaluating the unsteady flow routing model equations using the methodology suggested by Brunner (2016), the default model equation known as the 2D diffusion wave equation was used for the analysis. During the 2D model development of the study area, careful grid sizing was done, because the resolution of the spatial DEM data determines the grid sizes during the hydrodynamic model settings. Hence, for effective flood hazard evaluation, the concept of micro-scale flood modeling was used to obtain the flood depth and velocity relationships that aim to provide good results in terms of flood loss (Bermúdez and Zischg 2018). Since the study area is more in peri-urban and rural settings, farmlands, forest, and small settlements are predominant. Therefore, after evaluation of the most suitable grid size based on the building's arrangements (Gao et al. 2022), farmland characteristics, and computational time model, a 50-by-50-m grid meshing was adopted in this study. Although the impact of grid cell sizes ranging from 25 to 75 m has no significant impact on model performance (Ongdas et al. 2020).

### Estimation of dam breach parameters

Accordingly, to predict the peak flow as a result of dam failure due to excess inflow hydrograph, major breach geometrical parameters need to be determined. Several studies suggested varied numerical models, derived from historical trends of dam failures (Zhang et al. 2009). However, the developed models have different prediction uncertainties that are difficult to verify (Tschiedel and Paiva 2018). Therefore, the four dam failure models embedded in HEC–RAS 6.3.1 using a regression model were selected for the best breach parameter prediction of Gurara Dam in this study. Each of the models predicts varied breach parameters (width, slope, and time of breach formation) and tends to produce a different flow condition (Fig. 5b). A sensitivity analysis is required to select the appropriate breach parameter values to ensure the consistency of the flood hydrographs generated by the failed hydraulic structures. In addition, a realistic flood peak must be obtained at the targeted location downstream of the dam. To attain this goal, the model underwent calibration via the utilization of observed outflow from the spillway during a 24-h period and the application of Manning's coefficient, which was derived from the Land Use and Land Cover (LULC) analysis of the watershed. The validation of the model was conducted by comparing the inflow hydrograph, rainfall, and observed outflows over varying time intervals. Figure 5a shows the sensitivity analysis of the four selected predictive models. It shows that the MacDonald's methods are more sensitive to changes in reservoir attenuation capacity based on breach width, breach time, and breach slope, followed by Froehlichs and Xu's, and the least sensitive is the Von Thun and Gillette method. In terms of peak flows (Fig. 5b), MacDonald's method produced the highest peak,
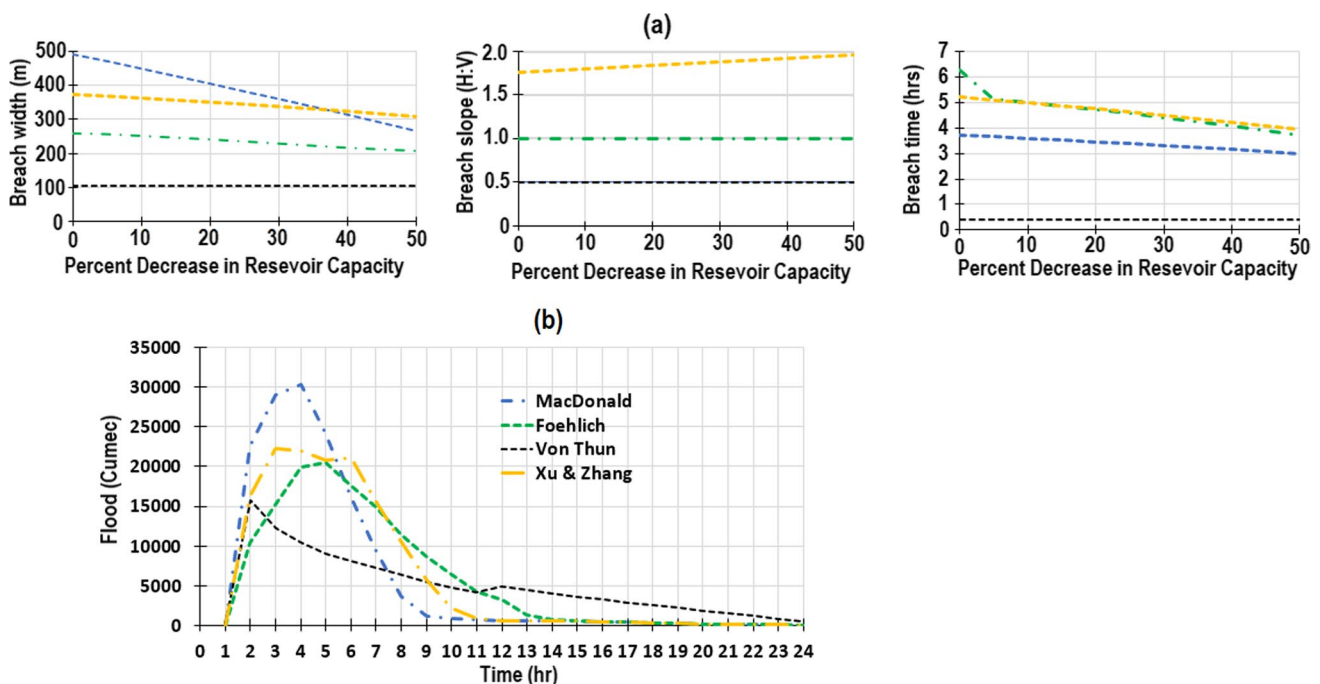


Fig. 5 Behavior of the four breach prediction methods **a** consistency test **b** peak flow

followed by Xu, Froehlich, and then the Von Thun and Gillette method. However, in both conditions, MacDonald's method proved to be the best model to use for dam breach modeling. Since the dam's storage capacity loss is a long-term progressive process, in a situation, where the sediment management is not adhered to, the dam becomes gradually vulnerable to failure during unprecedented flood events.

## Dam breach scenarios

To evaluate the dam attenuation capacity based on the dam breach conditions. The propagation of flood waves when failure occurs led us to assume that a flood could occur in the upper Gurara watershed due to the impact of LULC and climate change. Since the dam is made of rock fill (of the homogeneous type) and is a multi-purpose dam with multiple flood control structures, the most likely failure might be piping, not overtopping failure (Zhong et al. 2021). As mentioned in Sect. "HSPF Model", the four scenarios would be used to create a dam breach due to piping. In addition, we assumed 50% reservoir capacity, for each inflow scenario. It means that for scenario S1, it produces a maximum inflow of 2363 m3/s, which corresponds to a 56% increase in reservoir volume (686.4 million m$^3$); for scenario S2, it produces a maximum inflow of 1863 m3/s, which corresponds to a 44% increase in volume (633.6 million m$^3$), scenario S3, it produces a maximum inflow of 1072 m$^3$/s with a change in volume of 25.6% (552.6 million m$^3$); and for the last scenario (S4), it generates an inflow of 690m$^3$/s which corresponds to a 16% increase in reservoirs. A sudden change in volume due to excess inflow will stress the dam structure and subject it to rapid seepage, which will result in piping (Omofunmi et al. 2017). In this case, if continues, it will directly affect the safety of the dam structure as the severity of the flood waves increases with increase human activities at the upstream of the watershed.

Furthermore, the unsteady flow analysis was used for the hydrodynamic model of the study area, whereas the RAS Mapper was used to define the model geometry by assigning the dam characteristics, failure parameters, roughness constants, inflow data, computational time (24-h period was used throughout the analysis), boundary conditions, and initial conditions. Having successfully set the model based on the criteria outlined by Ghimire et al. (2022), the flood wave at the downstream was evaluated in terms of flood depth, velocity, and extent to estimate the flood hazard and vulnerability as the dam released the attenuated floods at varied inflow and storage capacity.

## Flood assessment

Recent studies produced hazard maps using the flood wave generated from the hydrodynamic model. We adopted the method used by Baky et al. (2020), which generated the hazard maps using the hazard curve from the literature. For the flood hazard map, we adopt the criteria used by Urzică et al. (2021). We created the vulnerability functions from the five LULC classes (forest, bare land, cropland, built-up, and agricultural land) using the depth-damage relationship, similar to Baky et al. (2020). However, in this case, we do not separate the LULC classes from their associated economic value. We combine them and analyze them to produce the vulnerability map for the flood areas. Although the vulnerability curve used in this study ranges from 0 to 4 m with flood depth and their corresponding vulnerability factor of 0 to 1 (see Table 3), we chose this approach, because our case study has similar characteristics to their study area, which is a mix of peri-urban and rural settlements with abundant farmland. Table 3 shows the criteria used to produce the two maps. For the projected land loss (for built-up and agricultural land only) derived from the result of the inundation due to dam failure on the downstream side of the watershed, the estimated land value in this study was based on a review of the National Emergency Management Agency assessment report (NEMA), a combination with the state government under the Kaduna State Geographic Information System (KADGIS), and direct interviews with local people. We set the estimated land value at N12,750 per cell for agriculture;

**Table 3** Adopted flood hazard and vulnerability index

| Classes | Flood hazard (m$^2$/s)[a] | Vulnerability index[c] | Description[b] |
|---|---|---|---|
| Very low | 0−0.3 | 0−0.15 | Little threat to human, animals, and crops |
| Low | 0.3−0.6 | 0.15−0.35 | Unsafe for mobility, children, short crops, and animals |
| Medium low | 0.6−1.2 | 0.35−0.60 | Unsafe for adult, elderly and major crops |
| Medium high | 1.2−2.0 | 0.6−0.75 | Unsafe to some public infrastructures, and agricultural lands |
| High | 2.0−4.0 | 0.75−0.9 | Damage buildings and contamination of arable lands |
| Very high | ≥4 | 0.9–1 | Unsafe for all building/settlement/cropland |

[a]Adopted from Urzică et al. (2021)

[b]Hussain et al. (2021)

[c]Baky et al. (2020)

N130,000 for settlements; N7650 for bare land; N3700 for cropland; and N9200 for the forest. We produced the flood risk map on the basis of these criteria (see Fig. 6).

# Results

## Simulated peak flows

After validating the hydrological model of the upper Gurara watershed, each of the four scenarios was simulated, keeping the same calibration parameters for each run. The model was set to simulate in hourly time steps. Using the 95th percentile statistical method, a maximum flood hydrograph with a duration of 24 h was selected for each scenario, as shown in Fig. 7. Since the historical rainfall duration at various intensities in the study area (which falls in the northern region) is less than 24 h (Tarhule and Woo 1998). Therefore, a 24-h model simulation based on the inflow scenarios was adopted. In each case, the maximum flood depth, flood velocity, duration and extent of flooding are extracted for further analysis.



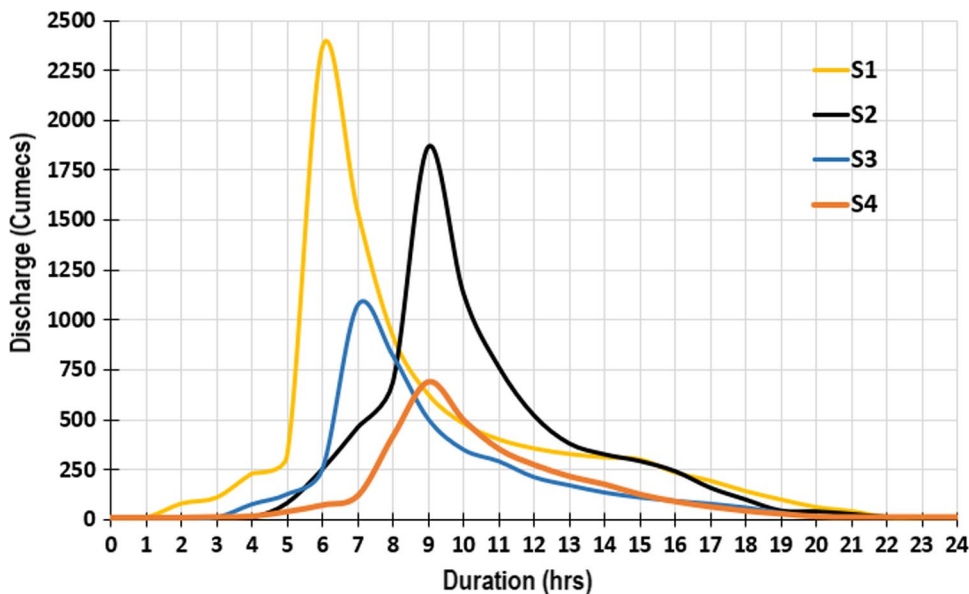Fig. 6 Maximum flood hydrographs at 95th percentile for the four scenarios S1, S2, S3, and S4
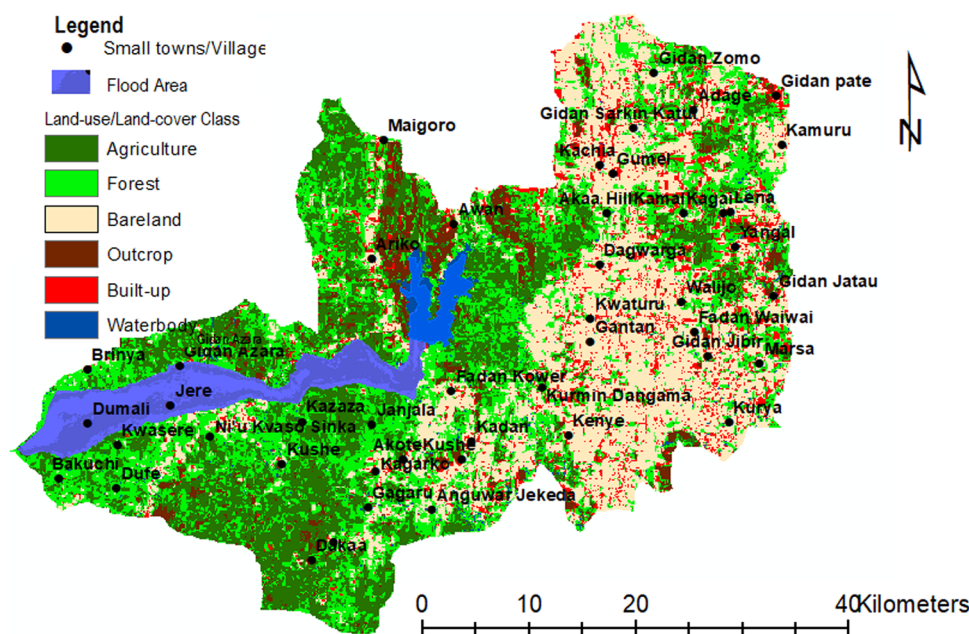


Fig. 7 Flood extent at the downstream of Gurara watershed

## Flood extent at the downstream of the watershed

The analysis of the dam breach under the four scenarios showed a flooded area of 274.6 $Km^2$ (approximately 27,460 ha), of which 83.69 $km^2$ (83,690 ha) is agricultural land, 145.06 $km^2$ (14,506 ha) is forest land, 25.85 $km^2$ (2585 ha) is bare land, 9.17 $km^2$ (917 ha) is cropland and 10.76 $km^2$ (1075 ha) is built-up land (Fig. 6). Although, the extent of flooding remains the same under all the four scenarios. This indicates that the extent of inundation is independent of the volume of the reservoir and the inflow of floodwater upstream of the dam. On the other hand, the breach parameters (breach width, slope and breach time) have no influence on the propagation of floodwater downstream of the catchment when the dam breaches. This is interesting, because it shows that the extent of flooding downstream of the catchment is a more or less constant phenomenon that allows for effective land use/land cover planning (LULC) within the identified area (27,460 ha). There is a need for targeted urban planning that responds to flood risks downstream of the dam. Although urban planning authorities are not sufficiently aware of the potential flooding in the event of a breach of the Gurara Dam, poor urban development due to informal practices and changing climatic conditions could increase the risk.

## Assessment of flood hazard

The simulated results of the dam breach were used to create the flood hazard map of the affected area by combining the flood velocity and depth in ArcGIS software for each scenario. It was found that the maximum and minimum flood hazard under scenario 1 were 38.9 $m^2$/s and 0.03$m^2$/s respectively, indicating "very high flood hazard" (observed near the rivers/catchments) as shown in Fig. 7. The affected areas (in $Km^2$) are matched with the corresponding flood hazard indices for each scenario based on the LULC classes of the catchment to assess the extent of flood hazard resulting from a hypothetical dam failure (Table 4). For scenario S1, it can be seen that 54.4% (5.4 $km^2$) of the built-up areas (which include Jere, Dumali and Gidan Azara villages) will be exposed to a "high flood hazard" (index between 2 and 4 $m^2$/s) in the event of a dam failure, while this value decreases to 4.4, 4.1 and 3.5 $km^2$ for scenarios S2, S3 and

**Table 4** Affected land-use/land-cover downstream by dam break with varied flood hazard and their extent under the four scenarios

| Scenarios | Flood Hazards | Hazard index range ($m^2$/s) | Land-use classes | | | | |
|---|---|---|---|---|---|---|---|
| | | | Agriculture (83.69 $Km^2$) | Forest (145.06 $km^2$) | Bare land (25.85 $Km^2$) | Outcrop (9.17 $km^2$) | Built-up (10.76 $km^2$) |
| S1 | Very low | 0−0.3 | 2.5 | 28.7 | 2.1 | 1.5 | 0.4 |
| | Low | 0.3−0.6 | 5.6 | 36.3 | 2.6 | 1.6 | 1.9 |
| | Medium low | 0.6−1.2 | 10.9 | 3.0 | 3.5 | 0.4 | 0.7 |
| | Medium high | 1.2−2.0 | 10.5 | 5.2 | 7.5 | 3.3 | 1.9 |
| | High | 2.0−4.0 | 14.0 | 10.8 | 1.2 | 1.1 | 5.4 |
| | Very high | ≥4 | 40.2 | 61.1 | 8.9 | 1.3 | 0.5 |
| S2 | Very low | 0−0.3 | 4.5 | 23.5 | 1.9 | 1.6 | 0.6 |
| | Low | 0.3−0.6 | 5.0 | 33.5 | 3.3 | 1.4 | 1.7 |
| | Medium low | 0.6−1.2 | 10.4 | 5.8 | 3.3 | 0.7 | 0.8 |
| | Medium high | 1.2−2.0 | 12.2 | 7.3 | 7.1 | 3.1 | 2.5 |
| | High | 2.0−4.0 | 13.6 | 17.9 | 1.7 | 1.3 | 4.4 |
| | Very High | ≥4 | 38.1 | 57.0 | 8.6 | 1.1 | 0.8 |
| S3 | Very low | 0−0.3 | 6.0 | 21.3 | 1.6 | 1.7 | 0.7 |
| | Low | 0.3−0.6 | 4.4 | 27.9 | 4.1 | 1.3 | 1.4 |
| | Medium low | 0.6−1.2 | 11.7 | 9.8 | 2.7 | 0.9 | 0.9 |
| | Medium high | 1.2−2.0 | 11.3 | 12.7 | 6.7 | 2.9 | 2.6 |
| | High | 2.0−4.0 | 13.1 | 26.9 | 2.4 | 1.5 | 4.1 |
| | Very high | ≥4 | 37.3 | 46.5 | 8.3 | 1.0 | 1.0 |
| S4 | Very low | 0−0.3 | 7.7 | 18.2 | 1.2 | 2.0 | 0.8 |
| | Low | 0.3−0.6 | 4.2 | 25.7 | 4.7 | 1.1 | 1.1 |
| | Medium low | 0.6−1.2 | 13.1 | 12.4 | 2.5 | 0.9 | 1.0 |
| | Medium high | 1.2−2.0 | 17.4 | 15.6 | 6.6 | 2.7 | 2.8 |
| | High | 2.0−4.0 | 11.9 | 30.6 | 2.8 | 1.7 | 3.5 |
| | Very high | ≥4 | 29.3 | 42.6 | 8.1 | 0.7 | 1.5 |

S4, respectively. However, the percentage of built-up areas exposed to "very high flood hazard" ($\geq 4$ m$^2$/s) is low compared to the values obtained for the "low" (maximum 1.9 Km$^2$), "medium" (maximum 0.7 km$^2$) and "medium–high" (maximum 1.88 km2) hazard index (Fig. 8). The LULC classes of agriculture, forest and outcrop areas were found to be most affected by a "very high" ($\geq 4$m$^2$/s) flood hazard.

Further analysis shows that agricultural lands that are closer to the river have a greater tendency to be in very high flood hazard situations with little control over the buildup. As the agricultural land mixes with the bare land, forest, and built-up areas, the impact is largely distributed among the major LULC classes, and the hazards are in multiple areas of the flooded zone, as shown in Table 4. For example, in all four scenarios, forest and agriculture are more affected by the flood, as it indicates that a minimum of 41% and 35.3% and a maximum of 49.1% and 44.6%, respectively, fall under "very high flood hazards". It indicates the potential of the flood to extremely disrupt the economic activities of the affected areas. It means that the flood propagation due to the breach of the dam, have consequences on the socio-economic activities of the people downstream, being that about 27.8 km$^2$ of the agricultural lands are utilized for irrigation purposes. In all the scenarios, the hazard condition increases toward the river and diminishes further away from it. To prevent flood hazards situations downstream, at least all planned development should be 1.5–2 km away from the river. While farmland can be allowed within a distance of 389 to 1500 m based on the hazard prevention criteria suggested by Mudashiru et al. (2022).

## Vulnerability assessment of the flooded area

The vulnerability maps for different scenarios were produced, as shown in Fig. 8. On the map, the respective vulnerability is: "very low" (0–0.15), "low" vulnerable (0.15–0.35), "medium low" vulnerable (0.35–0.6), "medium high" vulnerable (0.6–0.75), "high" vulnerable (0.75–0.9), and "very high" vulnerable (0.9–1) for different scenarios of dam break. In Fig. 9 , it is found that LULC vulnerability decreases as the inflow into the dam decreases. Nearly 22.3% of the total agricultural land area is "very high" vulnerable to S1 flood inundation. These areas are close to the Gurara River, and furthermore, they generally lie at low or average elevations. In addition, 30% of the total agricultural land area is "low" vulnerable to S1. Most of these areas are further away from the river floodplain. Significantly, the results in Fig. 9 illustrate the fact that the built-up land in the middle and side of the flooded area is much more vulnerable to flooding than any other area of the inundated site. This is due to the fact that the middle is very close to the Gurara River tailwater, one of the main rivers in the watershed. Furthermore, the area is an undulating zone, as observed in the DEM shown in
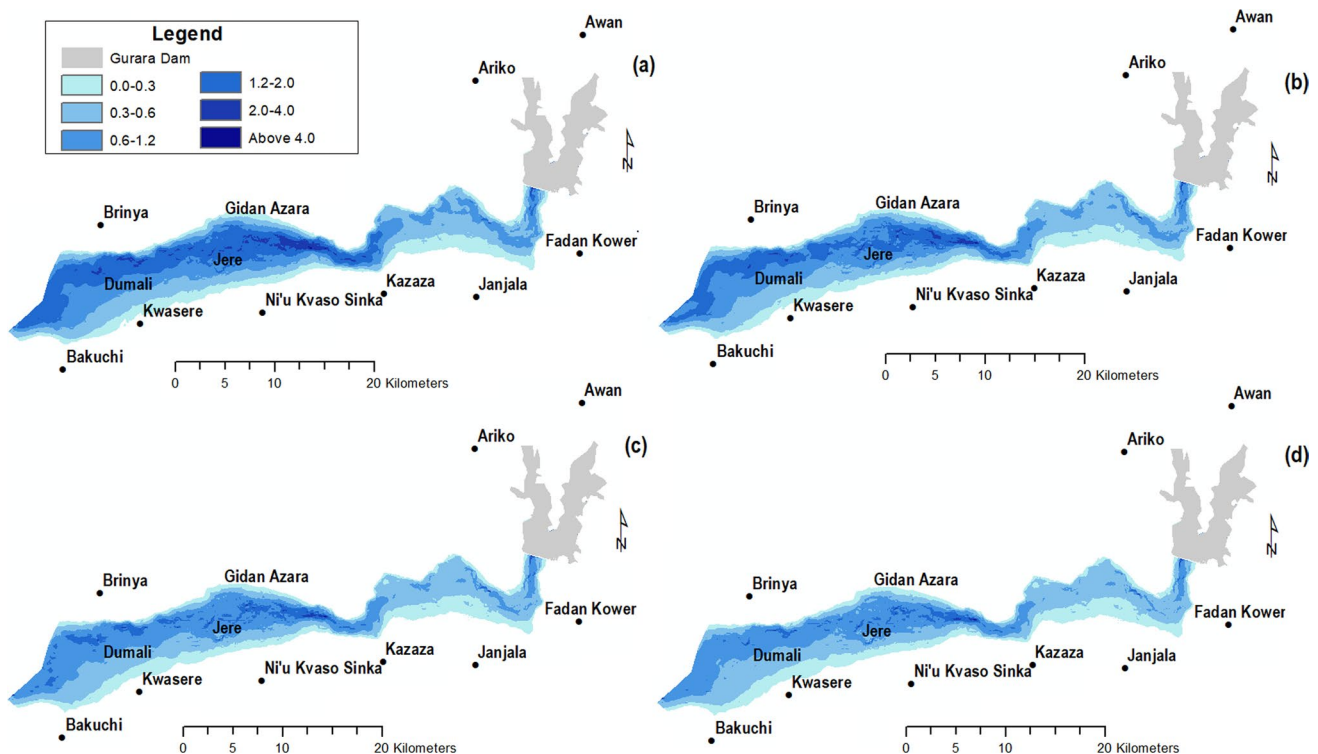


**Fig. 8** Flood hazards assessment maps of the four scenarios **a** S1 **b** S2 **c** S3 and **d** S4
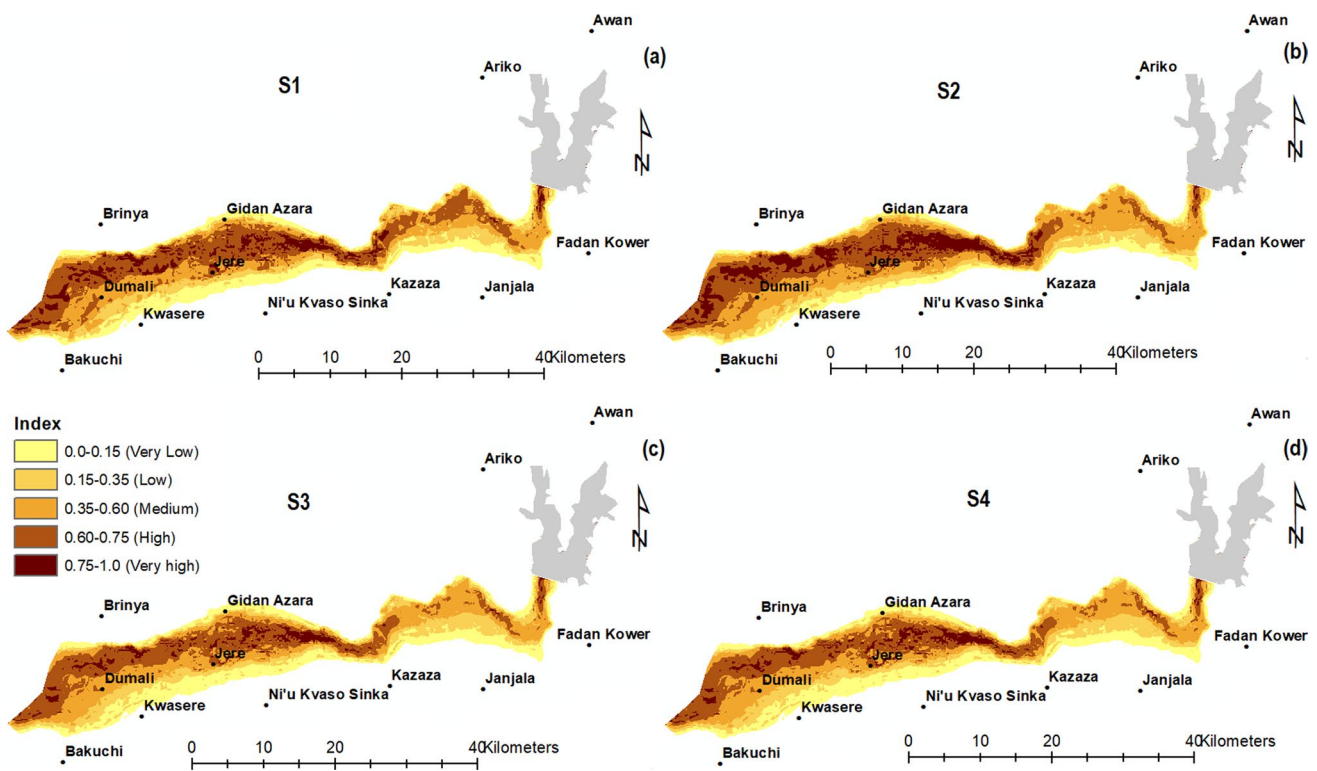
**Fig. 9** Vulnerability maps of the inundated areas downstream of the watershed under the four scenarios **a** S1, **b** S2, **c** S3 and **d** S4

Fig. 1. Consequently, the impact of flood damage would be higher in the middle and toward the outlet of the watershed than in any other flood sections. Note that this assumption is true for the same flood in terms of peak period and time to peak. However, forest land is more affected than agricultural land, as 33% of the total forest land flooded by the flood water is "very high" vulnerable, which is also dominant in the high elevations close to the dam and the low areas at the outlet.

Further analysis of the vulnerability map for other LULC classes, as shown in Table 5, illustrates that outcrop, bare land and built-up decreases with the decreases in inflow of water (S1–S4). In general, irrespective of any index of vulnerability, 16%, 12.2% and 9.1% of the total outcrop, bare land and built-up area is vulnerable to flooding in all scenarios. Now, if looking on the basis of vulnerability class, 56% of the total built-up area is "very high" vulnerable to flooding in Scenario S1, and reduced to 48.2% for Scenario S4. However, in Scenario S2 and S3 the percentage decreases to 4%. For outcrop, 26% is "very high" vulnerable to flood at scenario S1 and remains unchanged for all the scenarios. In addition, for bare land area, 46% is "very high" vulnerable to flooding for S1, but decreases to 44%, 39% and 36% for S2, S3, and S4 respectively. This decreasing trend is probably due to the location of the bare land areas as they are very close to the Gurara river and at the tail-water floodplains.

Considerably, outcrops and built-up areas "very low" vulnerable to flooding decrease gradually with decreased inflows upstream of the Dam (scenarios S1–S4). While bare land areas with "very low" are vulnerable to flooding, they increase with decreased inflows upstream of the dam. The area increases from about 26–32% from scenarios S1 to S4. These areas where bare land vulnerability with "very low" increases tend to be either close to the high elevation areas or far away from the Gurara River (Fig. 1). As a whole, distance from the river to any LULC classes affects the extent of vulnerability in the flooded area. However, the type of LULC classes is obviously a factor in this regard as they have different distribution and spatio-temporal conditions within the flooded areas, especially in a situation, where they are located at a low elevation and close to the Gurara river.

## Risk assessment of the flooded area

Figure 10 shows the expected risk map for the flooded area under different scenarios of dam break. Table 6 presents the areas of LULC classes with different levels of risk under different scenarios of dam break. It shows that the overall LULC classification with different classes of flood risk varies with each scenario. Though agricultural land areas with "low" and/or "medium" flood risks increased (from 28.3 to 32.1 km$^2$ for "low" and from 11.5 to 16.3 km$^2$ for "medium")

**Table 5** Vulnerability distribution across the land-use/land-cover under different scenarios

| Scenarios | Vulnerability | index range (m²/s) | Land-use classes | | | | |
|---|---|---|---|---|---|---|---|
| | | | Agriculture (83.69 Km²) | Forest (145.06 km²) | Bare land (25.85 Km²) | Outcrop (9.17 km²) | Built-up (10.76 km²) |
| S1 | Very low | 0−0.15 | 14.7 | 29.16 | 0.4 | 2.2 | 1.8 |
| | Low | 0.15−0.35 | 25.3 | 18.9 | 2.95 | 0.7 | 0.6 |
| | Medium low | 0.35−0.60 | 4.7 | 6.1 | 1.9 | 0.8 | 0.4 |
| | Medium high | 0.6−0.75 | 8.2 | 17.5 | 5.7 | 2.1 | 0.8 |
| | High | 0.75−0.9 | 12.1 | 25.6 | 2.8 | 0.8 | 1.1 |
| | Very High | 0.9–1 | 18.7 | 47.8 | 12.1 | 2.6 | 6.1 |
| S2 | Very low | 0−0.15 | 13.3 | 34.86 | 0.5 | 2.7 | 1.7 |
| | Low | 0.15−0.35 | 21.5 | 16.3 | 2.95 | 0.5 | 0.7 |
| | Medium low | 0.35−0.60 | 5.9 | 5.8 | 2.1 | 0.9 | 0.3 |
| | Medium high | 0.6−0.75 | 9.6 | 18.9 | 6.2 | 2 | 1.1 |
| | High | 0.75−0.9 | 11.4 | 24.7 | 2.7 | 0.7 | 1.2 |
| | Very High | 0.9–1 | 22 | 44.5 | 11.4 | 2.4 | 5.7 |
| S3 | Very low | 0−0.15 | 12.9 | 38.26 | 0.8 | 2.9 | 1.2 |
| | Low | 0.15−0.35 | 20.1 | 15.5 | 2.65 | 0.4 | 0.8 |
| | Medium low | 0.35−0.60 | 6.3 | 5.4 | 2.7 | 0.9 | 0.3 |
| | Medium high | 0.6−0.75 | 10.5 | 19.2 | 6.9 | 1.9 | 1.5 |
| | High | 0.75−0.9 | 9.6 | 23.8 | 2.7 | 0.5 | 1.5 |
| | Very High | 0.9–1 | 24.3 | 42.9 | 10.1 | 2.6 | 5.5 |
| S4 | Very low | 0−0.15 | 10.7 | 44.16 | 0.9 | 3.2 | 1.2 |
| | Low | 0.15−0.35 | 18.6 | 13.8 | 2.55 | 0.3 | 0.8 |
| | Medium low | 0.35−0.60 | 7.1 | 5.1 | 2.9 | 1 | 0.2 |
| | Medium high | 0.6−0.75 | 11.3 | 20.7 | 7.4 | 1.7 | 1.7 |
| | High | 0.75−0.9 | 7.8 | 21.1 | 2.8 | 0.4 | 1.6 |
| | Very High | 0.9–1 | 28.2 | 40.2 | 9.3 | 2.6 | 5.2 |

with the change in scenarios (from S1 to S4). The inflow of water decreases, and the "low" and "medium" risk conditions increase for flooded agricultural land areas. Steadily, the "high" risk zones under agricultural land decrease with a decrease in the inflow condition upstream of the dam (scenarios S1–S4). In addition, forest land area exhibits the same pattern as agricultural land area, even though forest land is the major LULC class that is most affected by the flood.

The forest land in the downstream direction, toward the tailwater of the Gurara river, is at risk for all the scenarios (Fig. 10). The reason why forest land areas with "low" and "high" flood risks decrease and increase, respectively, at the same time as the inflow changes. These areas transform from either high to medium or medium to low as the flood propagation decreases with the decrease in inflow from the upstream flood condition as presented in the four scenarios (S1–S4). Summarily, the significant change in elevation from the dam axis to the Gurara tailwater, which is about a 96-m difference in elevation (Fig. 1), is coupled with the meandering characteristics of the drainage system controlled by the complex terrain. Therefore, the flood velocity

characterized by the flood hazard map (Fig. 8) shows that the hazard is more significant within the identified areas (at the tail-water, close to the river, and abrupt change in elevation), and the vulnerability map (Fig. 9) presents the same conditions as earlier explained in sub-Sect. "Vulnerability assessment of the flooded area". The drainage system downstream of the catchment is complex, as it has varied levels of drainage area, slope, density, and relief, which amplified runoff and caused a sudden generation of floods. Hence, as the dam break results in the release of floodwaters with varied velocity and depth, when interacted with the condition of the drainage system, the flood hazard situation will increase, which will step up the level of vulnerability, and subsequently, the risk will change within both predominant LULC classes, the agriculture and forest land areas.

The risk for built-up, outcrop, and bare land shows varied changes for each scenario (S1–S4). Table 6 shows that bare land areas are most affected by "high" risk as compared to "low" and "medium" risk (7.1–12.1 km² for "medium,", 13.3–8 km² for "high," and 4.7–5.8 km² for "low"). Although for built-up land areas, the risk is
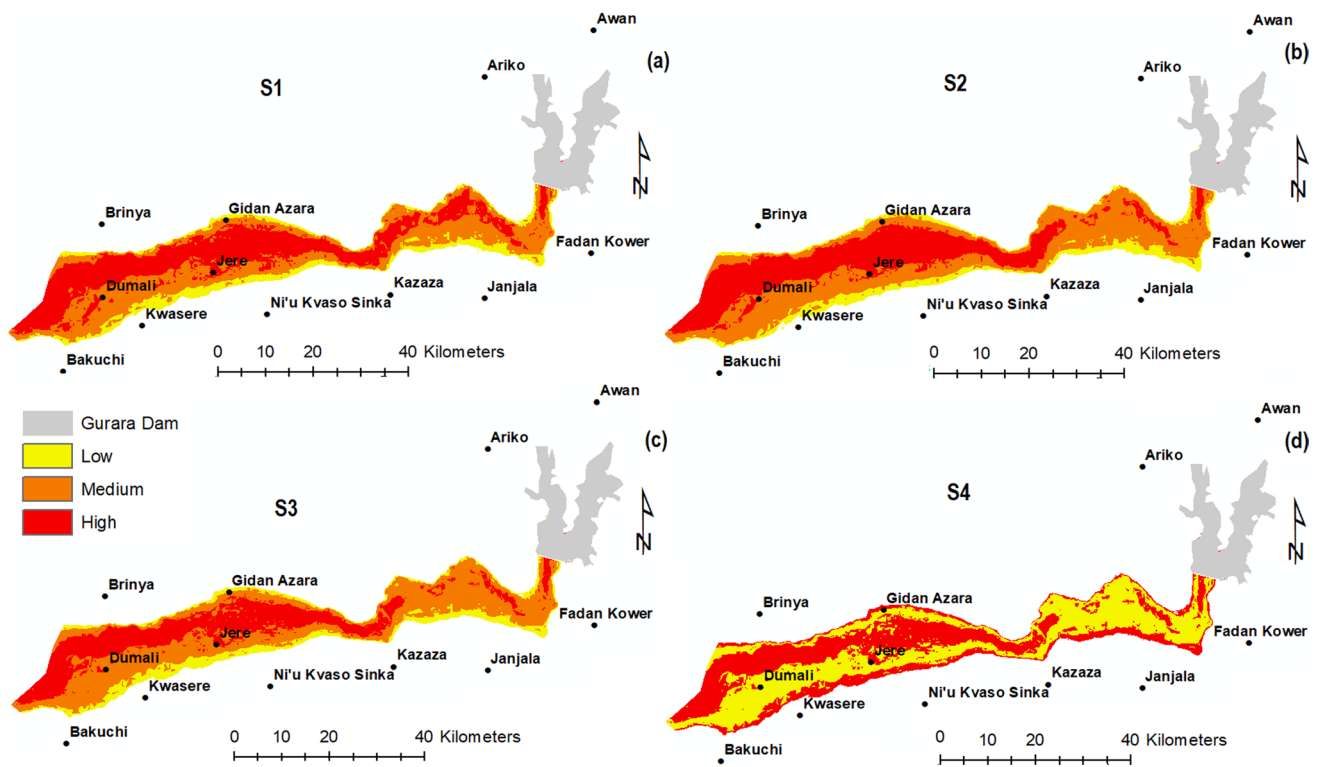
**Fig. 10** Risk maps of the inundated area downstream of the watershed under the four scenarios **a** S1, **b** S2, **c** S3 and **d** S4

**Table 6** Risk index in all the LULC classes under the four scenarios

| Scenarios | Risk | Land-use classes | | | | |
|---|---|---|---|---|---|---|
| | | Agriculture (83.69 Km$^2$) | Forest (145.06 km$^2$) | Bare land (25.85 Km$^2$) | Outcrop (9.17 km$^2$) | Built-up (10.76 km$^2$) |
| S1 | Low | 28.3 | 43.26 | 4.7 | 3.5 | 4.9 |
| | Medium | 11.5 | 25.4 | 7.9 | 3.6 | 0.8 |
| | High | 43.9 | 76.4 | 13.3 | 2.1 | 5.1 |
| S2 | Low | 29.1 | 49.16 | 4.9 | 3.3 | 5.1 |
| | Medium | 13.2 | 23.8 | 9.3 | 3.6 | 0.7 |
| | High | 41.4 | 72.1 | 11.7 | 2.3 | 5 |
| S3 | Low | 30.5 | 53.56 | 5.2 | 3.1 | 5.3 |
| | Medium | 14.7 | 22.1 | 10.6 | 3.6 | 0.5 |
| | High | 38.5 | 69.4 | 10.1 | 2.5 | 5 |
| S4 | Low | 31.2 | 56.06 | 5.8 | 2.98 | 5.9 |
| | Medium | 16.3 | 21.2 | 12.1 | 3.52 | 0.4 |
| | High | 36.2 | 67.8 | 8 | 2.7 | 4.5 |

significant at "low" and/or "high" risk levels, they tend to inter-change with the change scenarios S1–S4 (4.9–5.9 km$^2$ for "low," 5.1–4.5 km$^2$ for high," and 0.8–0.4 km$^2$ for "medium"). This implies that as the flood depth decreases (Fig. 8), the risk in the built-up area decreases. However, some of the built-up areas are far from the river, except for Jere Town, which is divided by the Gurara River. As

a result, the whole of Jere, with a total of 9912 inhabitants, falls within the "high" risk zone in all the scenarios. The reason could be the existence of undulating terrain within the town, with several tributaries that drain into the Gurara River tailwater and are connected on the left side of the Gurara River. Just before Jere town from the upstream side.

# Discussion

The results of this study show the hypothetical dam break of Gurara Dam under varied inflow conditions and its impact downstream of the Gurara watershed. Over the years, the watershed experiences various anthropogenic changes, as observed by the spatial analysis of the historical LULC over the span of 20 years. It was observed that a drastic change occurred on the LULC of the watershed after construction of the popular Gurara Dam. This is as a result of the socio-economic activities that commence immediately after the completion of the dam. About 6000 ha of land are dedicated for irrigation at the downstream, which is expected to generate 100,000 metric tons of food in three circles per year. On the other hand, there is rural to rural and rural to peri-urban migration during the same period as it encourages more people to move from their former location to the new rural and peri-urban areas that are mostly downstream of the dam and along the Gurara River and its tributaries. This was observed from the sudden change in the built-up and agricultural land from 2013 to 2020 (see Fig. 4) at the upstream of the watershed. The same situation was observed all within the watershed. In addition, the watershed is a center of tourism, and more people settle in peri-urban areas, such as Jere, Dufe, Dumalli, etc., at the upstream, and Kachia, Gumel, Maigoro, Ariko, etc. In addition, the topographic characteristics of the watershed encourage runoff, and an increase in impervious areas upstream (high elevation zones) is expected to increase the runoff situation that ends at the Gurara reservoir. Therefore, the impact of the LULC under increased rainfall conditions upstream of the watershed was evaluated to produce four scenarios (as 24-h inflow hydrographs): S1, S2, S3, and S4. This is to evaluate the dam's attenuation capacity and its control of excess runoff. It is important to note that the downstream of the watershed experiences flood events on a yearly basis (Ibrahim and Isiguzo 2009). After the construction of the dam, the floods experienced downstream decreased drastically. The question that remains unanswered is: what if, the inflow into the reservoir is beyond the dam's attenuation capacity, and what will be the consequences downstream? Hence, a hypothetical dam break analysis of the watershed was evaluated considering piping failure (Chen et al. 2019).

Piping failure was selected because of the type of dam, which is composite rock fill with multiple outlets (3 m diameter sluice gates, a 4200 $m^3$/s discharge spillway, and a 1.5-m-diameter penstock for power generation) that makes overtopping failure possible (Yilmaz et al. 2023). A sensitivity analysis of the four known correlation models for the prediction of the dam break parameters of the Gurara dam shows that MacDonald's method proved to be the best model for this study. The evaluation of the sensitivity analysis was based on the criteria used by Tschiedel and Paiva (2018). Most studies encourage the assessment of accidental floods from dam failure due to the disastrous downstream impact derived mostly from hydroclimatic and anthropogenic conditions (Azam and Li 2010; Mallakpour et al. 2019). A critical understanding of the preventive and adaptive measures in case of its failure. In Africa, this approach is not common nor implemented elsewhere within the continent (Munyai et al. 2019). Although there have been numerous dam disasters on the continent (Van Niekerk and Viljoen 2005; Fourie et al. 2022), in Nigeria, a lot of dams have failed but not all have been documented in the literature, resulting in damage to crops and destruction of property (Umaru et al. 2010; Ezugwu 2013).

The simulated model of the dam failure of Gurara dam follows the known procedure of the hydrodynamic model development (Sect. "Dam breach scenarios"). Considering the volume of water reserved by the dam, the large flood released as a result of the hypothetical dam failure downstream of the dam is disastrous and will impact LULC classes, the environment, and socio-economic activities (Latrubesse et al. 2020). With respect to the flood hazard maps produced from the flood propagation during failure, it shows that it has a different impact on the LULC classes. However, forests, agricultural land, bare land, and built-up areas are the most affected, as a large percentage fall within very high flood hazard conditions. In terms of flood propagation, all four scenarios (S1, S2, S3, and S4) produced the same flood extent with a varied flood hazard index. The influencing factor for the concentrated flood hazards (very high, high, medium, and low) is the significant elevation difference from the dam axis to the tailwater downstream. It is characterized by meandering rivers and their tributaries, which result in the sudden accumulation of floodwater and the efficient conveyance of floodwater in a short period of time (Fryirs 2017). These factors result in high flood hazards close to the rivers and their associated flood plains (see Fig. 7). The same condition was observed for the vulnerability map, as the flood hazards changed with the scenarios (S1, S2, S3, and S4), so did the vulnerability (Fig. 8). In general, the point of concern is that the vulnerable areas include the major peri-urban area known as Jere and its neighboring villages of Dumali, Gidan Azara, etc. For the agricultural areas, the proposed irrigation areas will be affected, which will render the effort of the Federal Authority in vain. About 100,000 metric tons of food will perish. This situation will produce a chain reaction in the socio-economic development of the country, the state, and the local community.

To evaluate the extent of risk, the risk maps of the study area were produced (Fig. 10). It shows a reasonable effect of flooding on the damages and risk in the event of dam

failure. The risk index was based on low, medium, and high risk. It was observed that 46–52% of the flooded area is potentially at high risk, but this changes with the decrease in inflow from upstream of the watershed. This implies that as the flood depth reduces (Fig. 8), the risk in the built-up, agricultural, forest, and bare land areas decreases. However, some of the built-up areas are far from the river, except for Jere Town, which is divided by the Gurara River. As a result, the whole of Jere, with a total of 9,912 inhabitants, falls within the "high" risk zone in all the scenarios. This calls for immediate action to curtail the disaster that is not known by the inhabitants of the downstream of the watershed that fall within the potential risk zones. Although a more realistic approach is required, it includes using existing projects to implement process-type tactics by adopting multilevel, multi-stressor, and geo-visualization methods to create awareness among the community in the Gurara watershed. This will help similar watersheds adopt sustainable management of their ecosystems and preserve the livelihoods of agricultural rural communities (Chauhan et al. 2020). On the other hand, local authorities should adopt the concept of flood risk preventive measures by creating awareness among rural dwellers and, at the same time, define the specific flood risk zones (Ali et al. 2022). They should impose stringent laws to discourage any form of human development that is detrimental to the ecosystem's survival and socio-economic impact if a disaster occurs from a similar or existing project near the community (Maganzani 2023).

## Conclusion

Dam-break floods have a devastating impact on ecosystems, environments, and socio-economic activities. These disasters are not communicated to at-risk residents or measured by authorities in many African countries like Nigeria. This study examines the hazards, vulnerabilities, and risks involved in a Gurara Dam breach downstream. It also demonstrates the dam's attenuation capacity and impact in the event of failure. The study uses four flood hydrograph scenarios derived from the simulated hydrologic model of the upper Gurara watershed as the inflow for the dam breach model. The study found that a total of 274.6 km$^2$ (27,460 ha) will be flooded, with agricultural land, forest land, bare land, cropland, and built-up land being affected. The flood hazard maps show that 54.4% of the built-up areas in Jere, Dumali, and Gidan Azara villages will be exposed to a high flood hazard in the event of a dam failure. In all four scenarios, forest and agriculture are significantly impacted by floods, with 41–49.1% and 35.3–44.6%, respectively, falling under "very high flood hazards". The vulnerability map showcases that 56% of the total built-up area is "very highly" vulnerable to flooding in Scenario S1, which decreases to 48.2% in

Scenario S4. In S2 and S3, percentage drops to 4%. LULC classes play a significant role in vulnerability conditions. They have different distribution and spatio-temporal conditions in flooded areas. Jere town and nearby villages are at high risk of flooding in all four scenarios as per the risk map. The current irrigation system has the ability to create a large amount of food, but is located in a risky area. If appropriate measures are not taken, the consequences may negatively impact the society, environment, and ecosystem. An adaptive plan and preventive measures are necessary to prevent a disaster in the Gurara watershed. This research examines the potential outcomes of a Gurara dam breach due to increased inflows from human activity and climate change upstream, and its effects on downstream areas. It highlights the need for authorities to assess potential floods in nearby communities near water structures, such as dams, dikes, and basins.

**Author contributions** Al-amin Danladi Bello and Abdullahi Sule Argungu conceptualized the manuscript and supervised the study, Aminu Tijjani Soron Dinki and Abdullahi Ibrahim wrote the main manuscript text, and Khalid Sulaiman, Abdulrazaq Salaudeen and Nura Idris prepared tables and figure. All the author reviewed the manuscript

**Data availability** Not applicable.

## Declarations

**Competing interests** The authors have not disclosed any competing interests.

## References

Abdessamed D, Abderrazak B (2019) Coupling HEC-RAS and HEC-HMS in rainfall–runoff modeling and evaluating floodplain inundation maps in arid environments: case study of Ain Sefra city, Ksour Mountain, SW of Algeria. Environ Earth Sci 78:586

Aboyeji OS (2016) Hydro-period dynamics of some inland valley agroecosystems in southwest Nigeria. Afr Geogr Rev 35:294–305

Açıl A, Aydın A, Eker R, Duyar A (2023) Use of UAV data and HEC-RAS model for dimensioning of hydraulic structures on forest roads. Croat J for Eng J Theory Appl for Eng 44:171–188

Ali A, Rana IA, Ali A, Najam FA (2022) Flood risk perception and communication: The role of hazard proximity. J Environ Manag 316:115309

Amini A, Bahrami J, Miraki A (2022) Effects of dam break on downstream dam and lands using GIS and Hec Ras: a decision basis for the safe operation of two successive dams. Int J River Basin Manag 20:487–498

Azam S, Li Q (2010) Tailings dam failures: a review of the last one hundred years. Geotech News 28:50–54

Baky MAA, Islam M, Paul S (2020) Flood hazard, vulnerability and risk assessment for different land use classes using a flow model. Earth Syst Environ 4:225–244

Bermúdez M, Zischg AP (2018) Sensitivity of flood loss estimates to building representation and flow depth attribution methods in micro-scale flood modelling. Nat Hazards 92:1633–1648

Bhattarai S, Parajuli PB, To F (2023) Comparison of flood frequency at different climatic scenarios in forested coastal watersheds. Climate 11:41

Bonsal B, Zhang X, Vincent L, Hogg W (2001) Characteristics of daily and extreme temperatures over Canada. J Clim 14:1959–1976

Brunner GW (2016) HEC-RAS river analysis system 2D modeling user's manual. US Army Corps of Engineers—Hydrologic Engineering Center, pp 1–171

Chauhan N, Shukla R, Joshi P (2020) Assessing impact of varied social and ecological conditions on inherent vulnerability of Himalayan agriculture communities. Hum Ecol Risk Assess Int J 26:2628–2645

Chen S-S, Zhong Q-M, Shen G-Z (2019) Numerical modeling of earthen dam breach due to piping failure. Water Sci Eng 12:169–178

Dam S, Jimoh O, Ayodeji O (2003) Water resources systems-hydrological risk, management and development (Proceedings of symposium 277 HS02b held during IUGG2003 at Sapporo, July 2003). IAHS Publ. no. 281, 2003. In: Page 277 *in* Water Resources Systems--hydrological Risk, Management and Development: Proceedings of an International Symposium (Symposium HS02b) Held During IUGG 2003, the XXIII General Assembly of the International Union of Geodesy and Geophysics: at Sapporo, Japan, from 30 June to 11 July, 2003. International Association of Hydrological Science.

Dasallas L, Kim Y, An H (2019) Case study of HEC-RAS 1D–2D coupling simulation: 2002 Baeksan flood event in Korea. Water 11:2048

Davenport FV, Herrera-Estrada JE, Burke M, Diffenbaugh NS (2020) Flood size increases nonlinearly across the western United States in response to lower snow-precipitation ratios. Water Resour Res 56:e2019WR025571

Elfeki A, Masoud M, Niyazi B (2017) Integrated rainfall–runoff and flood inundation modeling for flash flood risk assessment under data scarcity in arid regions: Wadi Fatimah basin case study, Saudi Arabia. Nat Hazards 85:87–109

Ezugwu C (2013) Dam development and disasters in Nigeria. Int J Eng Res Technol (IJERT) 2:960–977

Fourie A, Papageorgiou G, Blight G (2019) Static liquefaction as an explanation for two catastrophic tailings dam failures in South Africa. In: A. A. Balkema Publishers (ed) Tailings and mine waste 2000. CRC Press, LLC, USA, pp 149–158

Fryirs KA (2017) River sensitivity: a lost foundation concept in fluvial geomorphology. Earth Surf Proc Land 42:55–70

Gao H, Liu J, Lin P, Li C, Xiao Y, Hu G (2022) Pedestrian level wind flow field of elevated tall buildings with dense tandem arrangement. Build Environ 226:109745

Ghimire E, Sharma S, Lamichhane N (2022) Evaluation of one-dimensional and two-dimensional HEC-RAS models to predict flood travel time and inundation area for flood warning system. ISH J Hydraul Eng 28:110–126

Gouldby B, Sayers P, Mulet-Marti J, Hassan M, Benwell D (2008) A methodology for regional-scale flood risk assessment. In: Pages 169–182 in Proceedings of the Institution of Civil Engineers-Water Management. Thomas Telford Ltd

Guan M, Guo K, Yan H, Wright N (2023) Bottom-up multilevel flood hazard mapping by integrated inundation modelling in data scarce cities. J Hydrol 617:129114

Guo K, Guan M, Yu D (2021) Urban surface water flood modelling–a comprehensive review of current models and future challenges. Hydrol Earth Syst Sci 25:2843–2860

Ha H, Bui QD, Nguyen HD, Pham BT, Lai TD, Luu C (2023) A practical approach to flood hazard, vulnerability, and risk assessing and mapping for Quang Binh province, Vietnam. Environ Dev Sustain 25:1101–1130

Hussain M, Tayyab M, Zhang J, Shah AA, Ullah K, Mehmood U, Al-Shaibah B (2021) GIS-based multi-criteria approach for flood vulnerability assessment and mapping in district Shangla: Khyber Pakhtunkhwa, Pakistan. Sustainability 13:3126

Ibrahim HM, Isiguzo EA (2009) Flood frequency analysis of Figurara river catchmnet at Jere, Kaduna State, Nigeria. Sci Res Essay 4:636–646

Kim B, Sanders BF (2016) Dam-break flood model uncertainty assessment: case study of extreme flooding with multiple dam failures in Gangneung, South Korea. J Hydraul Eng 142:05016002

Kovalenko S, Brown CJ, Akan C, Schonning A (2022) An examination of extreme floods, effects on land-use change and seasonality in the lower St. Johns River Basin, Florida using HSPF and statistical methods. Environ Earth Sci 81:87

Kumar P, Debele SE, Sahani J, Rawat N, Marti-Cardona B, Alfieri SM, Basu B, Basu AS, Bowyer P, Charizopoulos N (2021) Nature-based solutions efficiency evaluation against natural hazards: Modelling methods, advantages and limitations. Sci Total Environ 784:147058

Latrubesse EM, Park E, Sieh K, Dang T, Lin YN, Yun S-H (2020) Dam failure and a catastrophic flood in the Mekong basin (Bolaven Plateau), southern Laos, 2018. Geomorphology 362:107221

Li W, Li Z, Ge W, Wu S (2019) Risk evaluation model of life loss caused by dam-break flood and its application. Water 11:1359

Lyu Z, Chai J, Xu Z, Qin Y, Cao J (2019) A comprehensive review on reasons for tailings dam failures based on case history. Adv Civ Eng 2019:1–18

Maganzani L (2023) Rivers and flood risk management in rural areas: some evidence from classical Roman law. Water Hist 15:125–159

Mallakpour I, AghaKouchak A, Sadegh M (2019) Climate-induced changes in the risk of hydrological failure of major dams in California. Geophys Res Lett 46:2130–2139

Martínez-Retureta R, Aguayo M, Abreu NJ, Stehr A, Duran-Llacer I, Rodríguez-López L, Sauvage S, Sánchez-Pérez J-M (2021) Estimation of the climate change impact on the hydrological balance in basins of south-central chile. Water 13:794

Moniruzzaman M, Thakur PK, Kumar P, Ashraful Alam M, Garg V, Rousta I, Olafsson H (2020) Decadal urban land use/land cover changes and its impact on surface runoff potential for the Dhaka City and surroundings using remote sensing. Remote Sens 13:83

Mudashiru RB, Sabtu N, Abustan I, Balogun W (2021) Flood hazard mapping methods: a review. J Hydrol 603:126846

Mudashiru RB, Sabtu N, Abdullah R, Saleh A, Abustan I (2022) Optimality of flood influencing factors for flood hazard mapping: an evaluation of two multi-criteria decision-making methods. J Hydrol 612:128055

Munyai RB, Nethengwe NS, Musyoki A (2019) An assessment of flood vulnerability and adaptation: a case study of Hamutsha-Muungamunwe village, Makhado municipality. Jàmbá J Disaster Risk Stud 11:1–8

Namara WG, Damisse TA, Tufa FG (2022) Application of HEC-RAS and HEC-GeoRAS model for flood inundation mapping, the case of Awash Bello Flood Plain, Upper Awash River Basin, Oromiya Regional State, Ethiopia. Model Earth Syst Environ 8:1449–1460

Nastiti KD, Kim Y, Jung K, An H (2015) The application of rainfall-runoff-inundation (RRI) model for inundation case in upper Citarum watershed, West Java-Indonesia. Proc Eng 125:166–172

Nkwunonwo U, Whitworth M, Baily B (2020) A review of the current status of flood modelling for urban flood risk management in the developing countries. Sci Afr 7:e00269

Omofunmi O, Kolo J, Oladipo A, Diabana P, Ojo A (2017) A review on effects and control of seepage through earth-fill dam. Curr J Appl Sci Technol 22:1–11

Ongdas N, Akiyanova F, Karakulov Y, Muratbayeva A, Zinabdin N (2020) Application of HEC-RAS (2D) for flood hazard maps generation for Yesil (Ishim) river in Kazakhstan. Water 12:2672

Oseke FI-e, Anornu GK, Adjei KA, Eduvie MO (2021) Predicting the impact of climate change and the hydrological response within the Gurara reservoir catchment, Nigeria. J Water Land Dev 129–143

Piciullo L, Storrøsten EB, Liu Z, Nadim F, Lacasse S (2022) A new look at the statistics of tailings dam failures. Eng Geol 303:106657

Polemio M, Lollino P (2011) Failure of infrastructure embankments induced by flooding and seepage: a neglected source of hazard. Nat Hazard 11:3383–3396

Rentschler J, Salhab M, Jafino BA (2022) Flood exposure and poverty in 188 countries. Nat Commun 13:3527

Salaudeen A, Shahid S, Ismail A, Adeogun BK, Ajibike MA, Bello A-AD, Salau OB (2023) Adaptation measures under the impacts of climate and land-use/land-cover changes using HSPF model simulation: Application to Gongola river basin, Nigeria. SciTotal Environ 858:159874

Sarchani S, Koutroulis AG (2022) Probabilistic dam breach flood modeling: the case of Valsamiotis dam in Crete. Nat Hazards 114:1763–1814

Serdeczny O, Adams S, Baarsch F, Coumou D, Robinson A, Hare W, Schaeffer M, Perrette M, Reinhardt J (2017) Climate change impacts in Sub-Saharan Africa: from physical changes to their social repercussions. Reg Environ Change 17:1585–1600

Song X-P, Hansen MC, Stehman SV, Potapov PV, Tyukavina A, Vermote EF, Townshend JR (2018) Global land change from 1982 to 2016. Nature 560:639–643

Swain SS, Mishra A, Sahoo B, Chatterjee C (2020) Water scarcity-risk assessment in data-scarce river basins under decadal climate change using a hydrological modelling approach. J Hydrol 590:125260

Tarhule A, Woo MK (1998) Changes in rainfall characteristics in northern Nigeria. Int J Climatol A J R Meteorol Soc 18:1261–1271

Tedla MG, Cho Y, Jun K (2021) Flood mapping from dam break due to peak inflow: a coupled rainfall-runoff and hydraulic models approach. Hydrology 8:89

Toosi AS, Calbimonte GH, Nouri H, Alaghmand S (2019) River basin-scale flood hazard assessment using a modified multi-criteria decision analysis approach: a case study. J Hydrol 574:660–671

Tramblay Y, Villarini G, Zhang W (2020) Observed changes in flood hazard in Africa. Environ Res Lett 15:1040b1045

Tschiedel AdF, Paiva RCDd (2018) Uncertainty assessment in hydrodynamic modeling of floods generated by dam break. RBRH 23. https://doi.org/10.1590/2318-0331.231820170074

Umaru A, Ogedengbe K, Omobowale M (2010) Structural failures of earth dams in Nigeria: a case study of Cham Dam in Gombe State. ARPN J Eng Appl Sci 5:47–52

Urzică A, Mihu-Pintilie A, Stoleriu CC, Cîmpianu CI, Huţanu E, Pricop CI, Grozavu A (2021) Using 2D HEC-RAS modeling and embankment dam break scenario for assessing the flood control capacity of a multi-reservoir system (NE Romania). Water 13:57

Van Niekerk H, Viljoen M (2005) Causes and consequences of the Merriespruit and other tailings-dam failures. Land Degrad Dev 16:201–212

Wijayawardana N, Abenayake C, Jayasinghe A, Dias N (2023) An urban density-based runoff simulation framework to envisage flood resilience of cities. Urban Sci 7:17

Xu Y, Zhang LM (2009) Breaching parameters for earth and rockfill dams. J Geotech Geoenviron Eng 135:1957–1970

Yilmaz K, Darama Y, Oruc Y, Melek AB (2023) Assessment of flood hazards due to overtopping and piping in Dalaman Akköprü Dam, employing both shallow water flow and diffusive wave equations. Nat Hazards, 117(1):979–1003

Zaborowski S, Kałuża T, Rybacki M, Radecki-Pawlik A (2023) Influence of river channel deflector hydraulic structures on lowland river roughness coefficient values: the Flinta river, Wielkopolska Province, Poland. Ecohydrol Hydrobiol 23:79–97

Zhang L, Xu Y, Jia J (2009) Analysis of earth dam failures: a database approach. Georisk 3:184–189

Zhong Q, Wang L, Chen S, Chen Z, Shan Y, Zhang Q, Ren Q, Mei S, Jiang J, Hu L (2021) Breaches of embankment and landslide dams-State of the art review. Earth Sci Rev 216:103597